DOI: 10.5604/01.3001.0014.4922

Volume 101 • Issue 2 • August 2020

Journal of Achievements in Materials and Manufacturing Engineering

International Scientific Journal published monthly by the World Academy of Materials and Manufacturing Engineering

Design and testing 3D printed structures for bone replacements

P.G. Ikonomov [a,*], A. Yahamed [b], P.D. Fleming [b], A. Pekarovicova [b]

[a] Engineering, Design, Manufacturing and Engineering Systems, Western Michigan University, 1903 Western, Michigan Ave, Kalamazoo, Michigan 49008, USA

[b] Chemical and Paper Engineering, Western Michigan University, 1903 Western, Michigan Ave, Kalamazoo, Michigan 49008, USA

* Corresponding e-mail address: pavel.ikonomov@wmich.edu

ABSTRACT

Purpose: 3D printing has shown enormous potential for building plastic products, including bone, organs, and body parts. The technology has progressed from visualization and pre-operation training to the 3D printing of customized body parts and implants. This research aims to create 3D printed bone structure from plastics and test the mechanical properties of the cortical and trabecular bone structures if they match the real bone structure strength.

Design/methodology/approach: We used Digital Imaging, and Communications in Medicine (DICOM) images from Computer Tomography (CT) scans to created external bone structures. These images' resolution did not allow the creation of fine trabecular bone structures, so we used 3D modeling software to engineer special 3D void honeycomb structures (with triangular, square, and hexagonal shapes). Another reason to design void structures is that the 3D printing of complex shapes without support materials is problematic. After designing and 3D printing of the 3D bone structures, their mechanical properties need to be tested.

Findings: 3D bone models, solid (cortical), and void (trabecular) bone structures were designed, 3D printed, and then tested. Tensile, bending, and compression testing was performed. Testing the mechanical properties of the honeycomb structures (triangular, square, and hexagonal) shows that their strength and modulus are higher than those of the real trabecular bones. The results show that 3D printed honeycomb structures mechanical properties can match and some cases exceeding the properties of the actual bones trabecular structures, while the sold structures have lower mechanical properties than the bone cortical structures.

Research limitations/implications: During the 3D printing experiments, we found that 3D printers, in general, have low resolution, not enough to print fine trabecular bone structures. To solve the existing 3D printing technology's insufficient resolution, we later designed and built an SLA (stereolithography) 3D printer with high printing resolution (10 micrometers). Another limitation we found is the lack of biocompatible materials for 3D printing of bone structures. Future research work is in progress formulating superior ink/resin for bone structures 3D printing. Further, clinical trials need to be performed to investigate 3D printed parts' influence on the healing of bone structures.

Practical implications: We found that the 3D void (honeycomb) structures will have an impact not only on building bone structures but also in engineering special structures for industrial applications that can reduce the weight, time, and the cost of the material, while still keep sufficient mechanical properties.

Originality/value: Designing and testing 3D printed bone models, solid (cortical), and void (trabecular) bone structures could replace bones. Design and test special void honeycomb structures as a replacement for cortical bone structures.

Keywords: 3D printing, Bone structure, 3D modelling, Testing, Mechanical properties

Reference to this paper should be given in the following way:

P.G. Ikonomov, A. Yahamed, P.D. Fleming, A. Pekarovicova, Design and testing 3D printed structures for bone replacements, Journal of Achievements in Materials and Manufacturing Engineering 101/2 (2020) 76-85. DOI: https://doi.org/10.5604/01.3001.0014.4922

BIOMEDICAL AND DENTAL ENGINEERING AND MATERIALS

1. Introduction

This research goal is to design, 3D print, and test mechanical properties of 3D solid (cortical) and void (trabecular) bone structures. While metal and ceramic implants have been used for years, plastics implants can increase patients' benefits to provide a better fit, comfortable wear, and biocompatibility. 3D printing (also called Additive Manufacturing) allows creating 3D printed plastic bone structure from personals Computer Tomography (CT) scans. The internal bone structure is porous, allowing blood and fluid to circulate, and other tissues grow inside the cavities. Therefore, to create an artificial plastic bone, it needs to have cortical external and trabecular internal structures. Though, before using 3D printed bones, the mechanical properties of the printed cortical and trabecular bone structures need to be tested to match the real bone strength. We used Digital Imaging, and Communications in Medicine (DICOM) images from CT scans to create a bone structure for 3D printing. The resolution of these images did not allow the creation of fine trabecular bone structures, so we used 3D modeling software to engineer a special 3D void structure. Another reason to design such a structure is the nature of 3D printing that cannot print complex shapes without support materials; if support material is used, it cannot be removed easily.

1.1. Designing of bone structures from DICOM images

DICOM images from CT scans were used to create a bone structure for 3D printing. The CT scanner uses X-rays passing through the body to create thinly sliced pictures of bones and organs. Images are taken layer by layer of the body, creating sections X, Y, and Z slices. Each pixel of the image is assigned a known value representing the relative location in the body. CT scans can find cysts, abscesses, infection, tumors, aneurysm, lymph nodes, foreign objects, bleeding, kidney stones, blockages, liver diseases, broken bones, and more [1].

The significant advantages of CT scans are that they generally have lower costs and only take about five to ten minutes to generate the data. Also, CT can scan even if a person has objects in them, such as metal implants, while with a Magnetic Resonance Imaging (MRI) scan, you cannot have any metal. Although CT scans can pick up both organs and bones, the CT has a better resolution of bone structures, while MRI scans can have higher detailing of soft tissue areas [2].

1.2. Engineering 3D void structure

As mentioned above, the resolution of DICOM images did not allow the creation of fine trabecular bone structures. Even if we could obtain high-resolution micro CT scan images and create fine trabecular bone structures, 3D printing technology cannot print complex shapes without support materials. When support material is used, it is not possible to remove it from the inside voids. Therefore, we decided to engineer a special 3D void structure that can be 3D printed without support structures. 3D structures were designed with hexagonal, triangular, and square interconnected voids throughout the entire body. These structures mimic the extracellular matrix properties (ECM) of the trabecular bone. We chose these structures, well known in specific high-end applications (e.g., aerospace), for their capability to provide high strength while reducing weight.

1.3. Selective laser sintering (SLS)

Selective laser sintering (SLS) works by fusing superfine powder material (plastic, ceramic, or metal) with a high-power laser. Depending on the powder used, the particles are sintered or melted to bind them together. The system has two chambers with pistons; one is for the powder supply; the second is for moving the working plate, see Figure 1. The powder supply piston moves up to add material, then the roller disperses and levels a thin layer of powder on the top of the working plate.

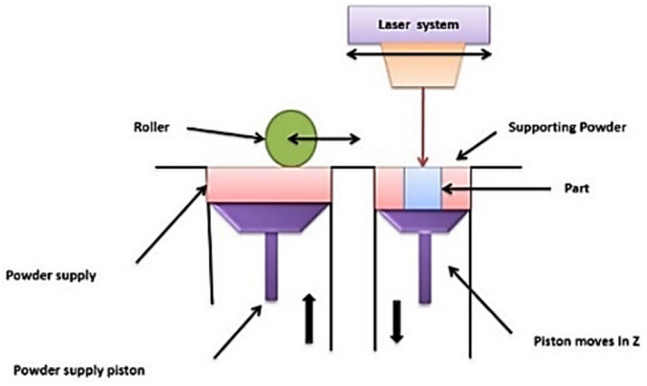

Fig. 1. Selective Laser Sintering

The laser system traces a predefined pattern (X and Y directions) on the layer, and the powder particles are fused from the heat to create the first layer. Then for the next layer, the working plate is dropped one step equal to the thickness of the layer on vertical Z direction. Again the powder supply piston brings fresh material, the roller disperses it on the top of the previous layer, and laser traces over the pattern on the new layer. This process is repeated multiple times until the part is completed. Finally, the part is removed from the working chambers, and additional operations like rebinding and melting can be performed.

1.4. Fused Deposition Modeling

Fused Deposition Modeling (FDM) is the most common technique that works by depositing a molten plastic filament (work similar to a hot glue gun) to construct a 3D printed piece, see Figure 2. The thermoplastic filament is pulled from spools, melts inside the heat extrusions heads with nozzles, and deposits the material on a build platform to solidify and form a layer. The nozzles are mounted on

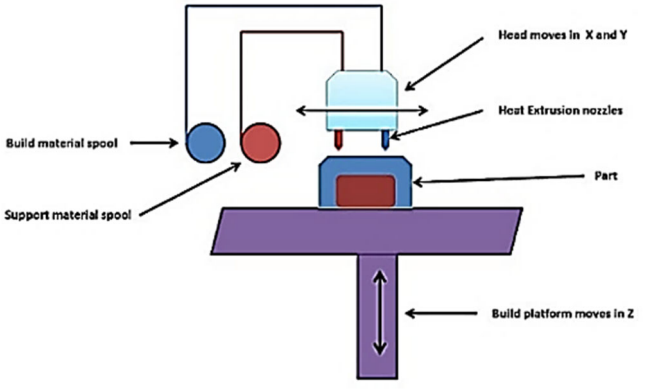

Fig. 2. Fused Deposition Modelling

a motion platform that controls the path for delivering the molded materials on the layer plane. The next layer is created on top of the previous one after the platform is dropped one step equal to the thickness of the layer on the vertical Z direction. This process is repeated multiple times until the part is completed. Finally, the part is removed from the working chambers, and additional operation like removing support material is performed.

1.5. Material jetting

Material jetting works very similar to inkjet paper printing. Instead of ink the multiple nozzles head deposit ultra-violet (UV) curable material on a flat building platform, see Figure 3.

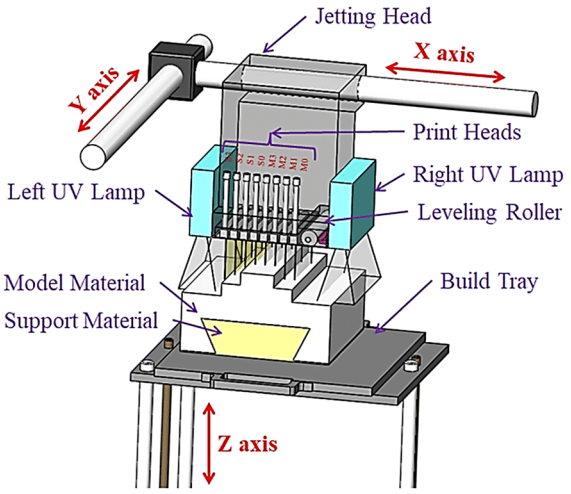

Fig. 3. PolyJet 3D printing [3]

The UV light source, which follows the printing head's movement, cures the layer that instantly solidifies. If there is a need for support materials, it is deposited and cured together with the core material. The flat building platform is then dropped one step equal to the thickness of the layer on vertical Z direction. The subsequent layers are deposit on the top of the previous layers. This process is repeated multiple times until the part is completed [4].

2. Methodology

2.1. 3D printing of the 3D shaped bone structures

To create 3D bone shapes, they need to be modeled from actual CT scan bone models. OsiriX and 3Dslicer software

were used to create 3D models. Initially, we used OsirX, but later we found that 3D slicer gives more flexibility to develop complex models from CT scans. CT scan from actual body parts was used to create multiple 3D printing models, see Figure 4 [5]. DICOM images from the CT scans were imported and arranged in X, Y, and Z-axis cross-sections cutoffs. The main stage, so-called Image segmentation, includes the following steps: import DICOM format images, select Region of Interest with Thresholding, Region growing, and Edge detection.

This process allowed selection only the bones needed to make into a 3D model. The higher the quality of CT scans, the higher the quality of the produced model. Finally, after the 3D model is produced, a triangulated surface mesh is created and exported to STL (Standard Triangle Language or Standard Tessellation Language) or other file formats. The selection process is not perfect and picks another part of the body that needs to be refined in MeshLab [6] software.

MeshLab, opens source 3D meshes software, was utilized to refine the models, allowing the mesh quality for better surface models, see Figure 5. MeshLab was used to check the polygon count, cleaning, healing, inspecting, and editing the mesh quality from imperfections like missing polygons, directions of the normal, and consistency of the surface form, fill small holes, and to smooth the surfaces.

The 3D bone models were imported and 3D printed with MakerBot Replicator 2X using ABS, PVA, and PLA materials. Several bones, such as a vertebra, see Figure 6 and femur structure [5] were 3D printed. Some models were scaled down to fit in the working volume of the 3D printer. Samples of 3D solid and void bone structures were tested to ensure that different 3D printing materials can meet functional mechanical properties.

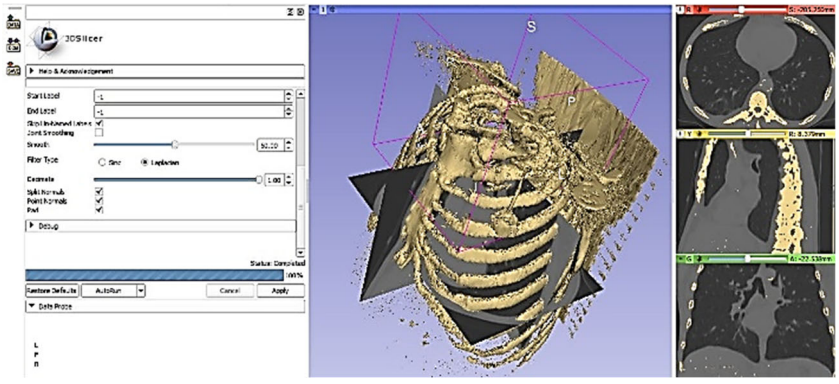

Fig. 4. 3D model created after segmentation in 3Dslicer

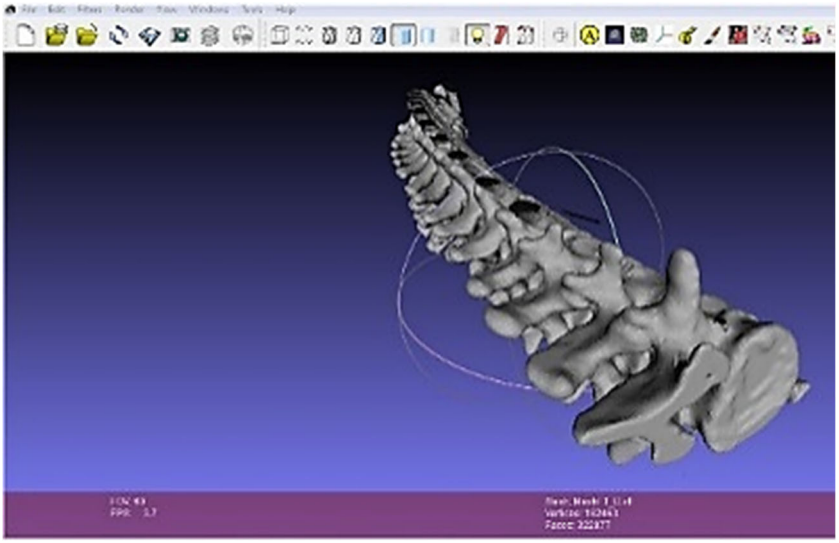

Fig. 5. 3D model cleared with Meshlab

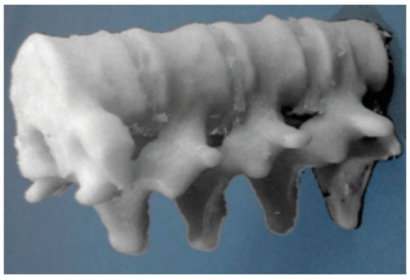

Fig. 6. 3D printed vertebra bone

Mechanical properties of 3D printing samples with 100% infilled for materials ABS, PLA, ULTEM9085, PA2200, Digital ABS™ were tested and shown in the result section of this paper.

2.2. 3D printing of void structure sample

Bones have a cortical bone (compact) and trabecular (spongy) structures. After testing the mechanical properties of 3D printed cortical bones, samples representing trabecular parts of the bone need to be tested as well. Void bone structures that mimic the spongy bone structure of the real one were tested in this research.

Engineering trabecular bones void structure with complex external and internal organic surfaces is almost impossible using traditional manufacturing technics like machining, casting, plastic extrusion, and others. One of the main reasons is that it is difficult to build small void structures that can't be accessed with common tools and machines. While it is possible to extrude, glue, cast parts with hollow structures, they tend to be linear or circular shapes, with relatively big sizes, which is suitable for industrial purposes but makes them unsuitable to use in biomedical applications, such as bone structures.

So far the solid objects, sheet or solid metal, or fixtures like nails and screws have been used to fix the broken bone structures, but they can't become an integrated part of new or existing bones since the tissue will not grow on them, blood and plasm will not pass through them as well, and they can be heavy. Furthermore, these materials/tools are difficult to customize and are built on the base one fit it all. Each human body part, including bones, is unique, so the existing technology is no match for nature when you want to create individual body parts. With the advance of the technology, 3D models of individual bone can be created from CT or X-Ray scans, but making them persona fit is extremely difficult and expensive.

3D printing drastically changed the landscape of the production of complex shape parts. Now we have technology that could produce 3D objects to be the exact copy of the original or precisely fit other parts. Fixing human bone can be customized to fit an individual and maintain tight details, tolerances, and lower costs.

One of the 3D printing main issues is that only a few materials are approved to be used inside the human body, and parts/bones produced with this technology are still not thoroughly tested.

As mentioned above, even if a solid object is 3D printed, it still can cause a few problems. For that reason, void based structure mimicking the human bone internal structures need to be investigated. Several biocompatible types of materials were tested that can be 3D printed and eventually used as bone structure replacements. The honeycomb structures models with triangular, square, and hexagon 3D shapes were engineered using Solid Works, Autodesk 3D Studio Max, and Meshlab 3D software, see Figures 7, 8, and 9.

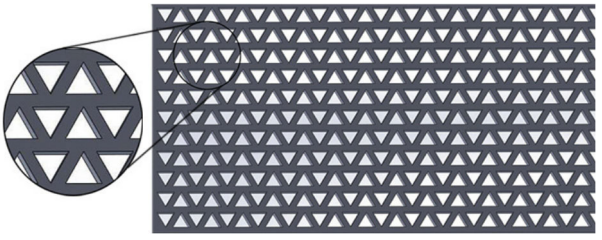

Fig. 7. Triangular structure

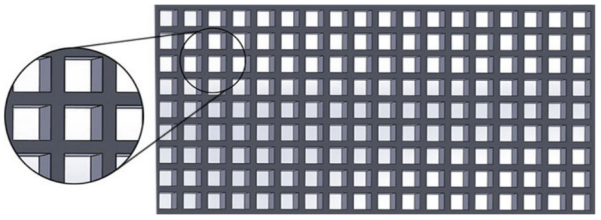

Fig. 8. Square structure

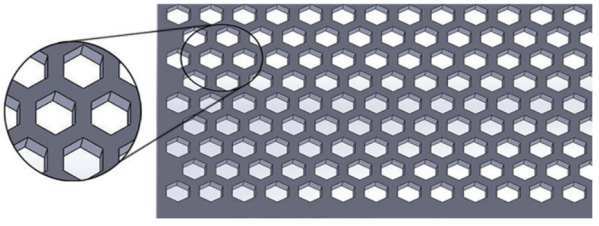

Fig. 9. Hexagonal structure

The voids' size was designed to match the average size of spongy voids of the real bones. The triangular structure contained 16.8% void, the square structure 17.2% voids, and the hexagon structure 7.4% voids. ULTEM9085, PA2200, Digital ABS™ materials were used for 3D printing.

Not all materials were used for the void structures, like ones for the solid bone structures, because we cannot print samples with high enough resolution to make all the small voids.

3. Results and discussions

3.1. 3D printing layers' data model preparation

Several steps are common for all 3D printing methods. At first, the 3D model of the desired part needs to be prepared using solid modeling CAD software. Then the model needs to be converted to STL file format used by 3D printers. The STL is the most common 3D printing file format that can represent complex surface geometry. The advantages are scalability and a decent quality of the surface. The STL file is then sliced to layers, using 3D slicer software. Each slice contains information about the 2D path that needs to be traced to complete the layer. The thickness and numbers of the layers depend on the design quality and a particular 3D printer setting.

Stacking layers on top of each other are repeated to create a part. The part quality can be tuned by increasing the number of polygons (triangular surface) that build the STL geometry and decrease the thickness of the layers. While still not widely used, new standard file formats provide more options to create better quality parts. Other standard 3D printing formats are OBJ, AMF, and 3MF, include additional information about geometry, color, texture, and material.

3.2. Testing the mechanical properties of the solid samples

Five different plastic materials, polyamide (PA2200), acrylonitrile butadiene styrene (ABS), polylactic acid (PLA), polyetherimide ULTEM9085, and digital ABS™ were 3D printed and tested using a tensile testing machine. PA2200 was 3D printed with SLS 3D printer model EOS P 396 SLS. ABS samples were printed with FDM 3D printer model Makerbot 2X, PLA samples were 3D printed with Ultimaker Type A Series 1, and ULTEM9085 samples were 3D printed with FDM 3D printer model Fortus 400 MC. Digital ABS™ samples were 3D printed using PolyJet Technology with binder jet 3D printer model Stratasys 500 Objet Connex3. After 3D printing, samples for tensile tests, compression tests, and bending tests were performed using tensile testing machine MTS Bionix Servohydraulic Test Systems-Model 370.02.

Tensile strength test

Five samples from each material with 100% infill were 3D printed and tested on the MTS machine with a speed of 0.2m/s at ambient temperature 20°C. The least-squares regression of the experimental data using a quadratic polynomial is shown in Figure 10. The shapes of stress-strain curves indicate brittle structures that do not exhibit any radical changes in elongation preceding the breaking. The results from tensile testing of 3D printed materials show that PLA has the highest Young's modulus and tensile strength from all samples. Digital ABS™ has the second-highest Young's modulus and tensile strength.

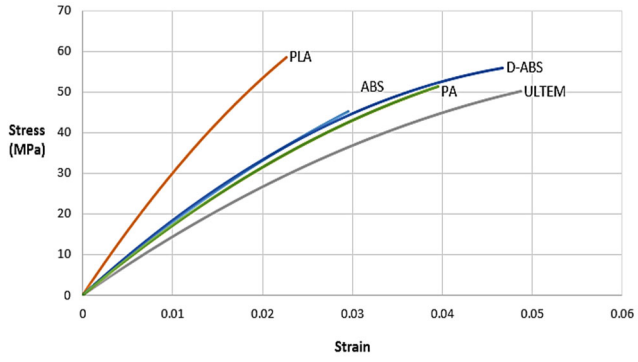

Fig. 10. Tensile stress-strain calculated from least squares fit to tensile data for the materials

ULTEM9085 has the lowest value for Young's modulus, and ABS has the lowest value for tensile strength. According to some research, cortical bones have a compressive strength in the range of 131-224 MPa, and Young's modulus ranging from 17 000-20 000 MPa, while compressive strength and Young's modulus for trabecular bones are 5-10 MPa and 50 -100 MPa, respectively [7]. The results show that 3D printed samples have strength and modulus less than the compact bone criteria, but they exceed the requirements of the trabecular bone.

Compression strength test

Cubic samples with sizes 25.4x25.4x25.4 mm from each material with 100% infill were 3D printed in two directions horizontally, along X-axis and vertically along Z-axis.

The results from testing of 3D printed materials show PLA has the highest compressive modulus in the X-direction and the second compressive strength in the Z-direction. Digital ABS™ has the highest compressive strength in the Z-direction and the second-highest compressive modulus in the X-direction. PA2200 has the lowest compressive modulus in the X-direction, and ABS has the lowest compressive strength in the Z-direction, Figures 11 and 12.

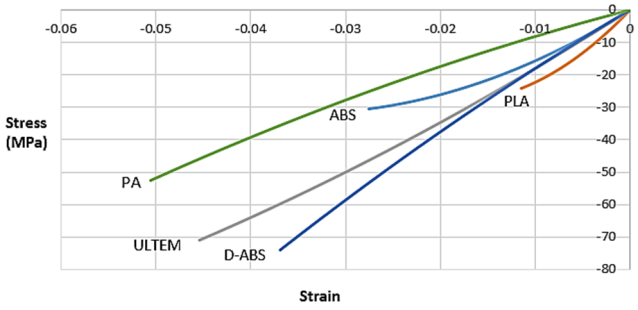

Fig. 11. Compressive stress-strain calculated from fits for printing in X direction

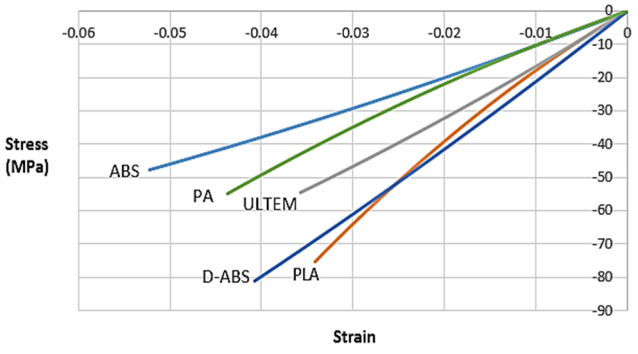

Fig. 12. Compressive stress-strain calculated from fits for printing in Z direction

According to some research, compressive modulus values of human trabecular bones range from 1 MPa to 5 000 MPa, with strength values ranging from 0.10 MPa to 27.3 MPa [8].

Bending tests

Bending testing evaluates the reaction of materials to realistic loading situations [9]. Human bone is loaded by a complex combination of forces, including tension, compression, and shear. Bending tests were performed by measuring the bending of a beam sample set on three points bend fixture, according to the ASTM D790 standard. The test parameters were the support span, loading rate, and the determined deflection. Figure 13 clearly shows the concave shape of bending stress-strain curves for all materials except Digital ABS™, which has a convex shape.

The results from testing 3D printed materials show that PLA has the highest flexural modulus value, ULTEM9085 is the second-highest value, and PA2200 is the third. For more details on testing the mechanical properties of these materials, refer to our previous publication [10].

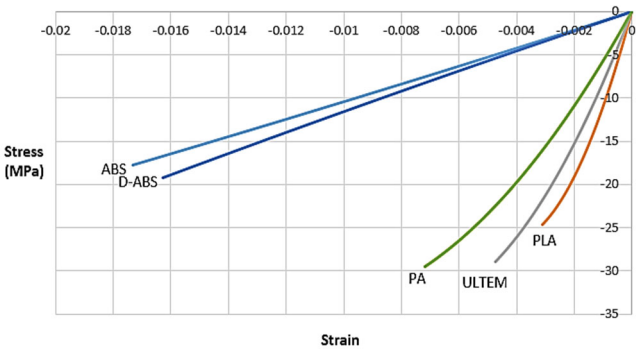

Fig. 13. Stress-strain calculated from fit to bending data at 100% infill for the materials

3.3. Testing the mechanical properties of the honeycomb structure samples

Printing honeycomb structure poses several challenges regarding the geometry complexity and biocompatibility. It is not accessible to 3D print samples with high enough resolution to make all small voids, as explained above. It is also essential to use proper bone replacement material that provides biocompatibility with sufficient stiffness and strength.

The plastics selected for testing were ULTEM9085, PA2200, and Digital ABS™. Polyetherimide ULTEM9085 is a biocompatible material used in tissue engineering scaffold for bone regeneration [11], and polyamide PA2200 was used in medical applications to build compressed structures for scaffold supporting [12]. Digital ABS™ is not a biocompatible material, but it was used as a reference for comparison with other polymers since 3D printer Stratasys Objet 500 Connex3 provides high enough resolution.

All testing samples were created following the standards, and the same MTS testing machine was used as described earlier for solid samples. ULTEM9085, PA2200, and Digital ABS™ samples with triangular, square, and hexagonal structures were 3D printed and tested. For comparison, solid samples from the same materials were printed and tested as well. Tests were performed on at least five samples for each of these materials.

Tensile strength tests of the honeycomb structure

Tensile tests were performed on at least five samples for each ULTEM9085, PA2200, and Digital ABS™ material 3D printed with triangular, square and hexagonal structures, see Figures 14, 15, and 16. For reference, solid samples were printed from the same materials and compared with the honeycomb structures.

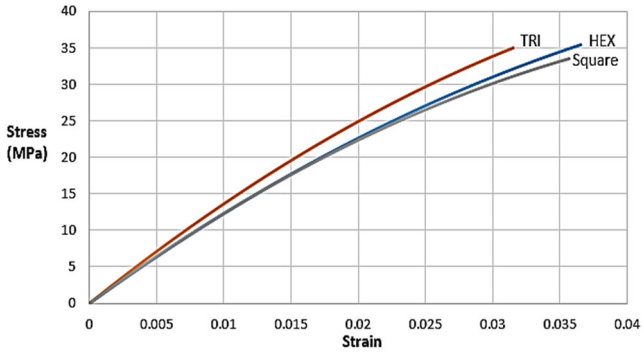

Fig. 14. ULTEM9085 structures stress-strain calculated from tensile data

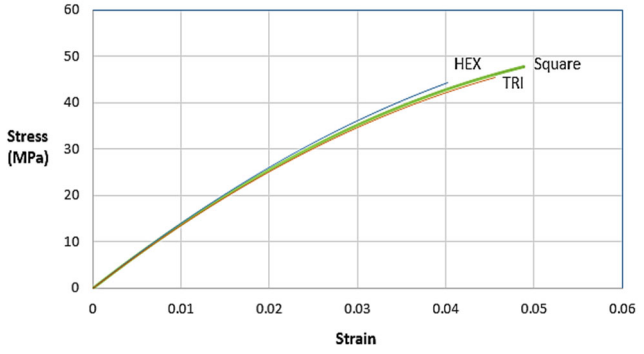

Fig. 15. PA2200 structures stress-strain calculated from tensile data

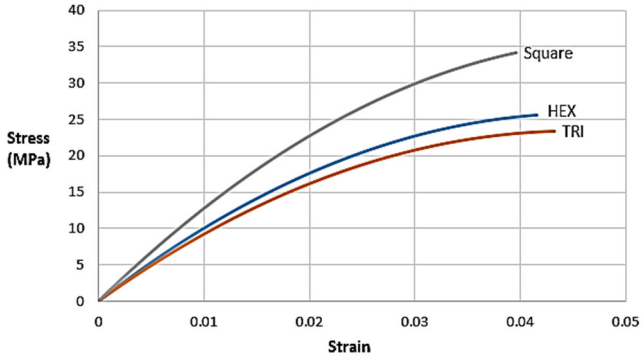

Fig. 16. Digital ABS™ structures stress-strain calculated from tensile data

The results from the tensile testing show that ULTEM9085 triangular structure has the highest Young's modulus, while the hexagonal structure has the lowest values. All the honeycomb structures show lower tensile strength test values than solid structures. In the case of PA2200, the hexagonal structure has the highest value of Young's modulus, while the triangular structure has the lowest, though the difference is relatively small. Tensile testing of Digital ABS™ shows that square structure performed the best with tensile strength and for both Young's modulus highest values, while the triangular structure has the lowest values for both. The relationship between tensile strength and Young's modulus is well correlated.

Compressive strength tests of the honeycomb structure

Compressive tests were performed on five samples for ULTEM9085, PA2200, and Digital ABS™ materials with triangular, square, and hexagonal structures. For reference, solid samples were also 3D printed from the same materials and compared with these honeycomb structures, see Figures 17, 18, and 19.

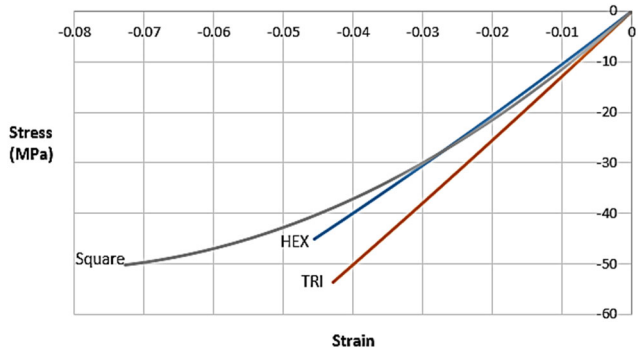

Fig. 17. ULTEM9085 structures stress-strain calculated from fit to compression data

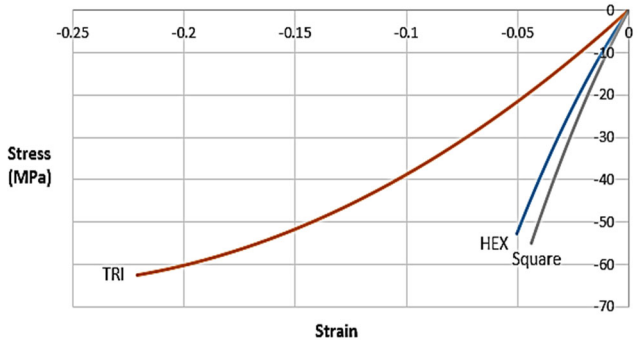

Fig. 18. PA2200 structures stress-strain calculated from fit to compression data

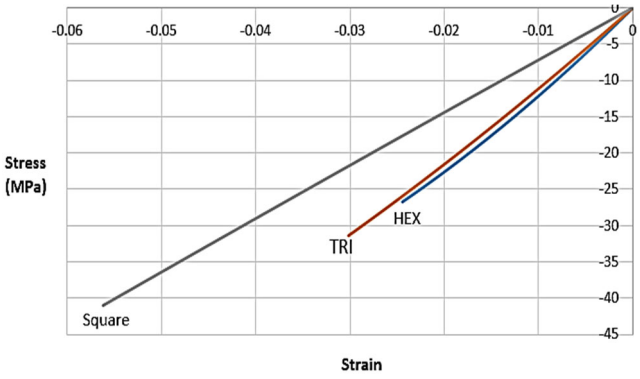

Fig. 19. Digital ABS™ structures stress-strain calculated from fit to compression data

The tensile testing results show that the ULTEM9085 triangular structure has the highest Young's modulus, while the hexagonal structure has the lowest values. In the case of PA2200, the square structure has the highest value of compressive modulus, while the triangular structure has the lowest, and all three structures show the same tensile strengths. Compressive testing of Digital ABS™ shows that hexagonal structure performed the best with the highest compressive, while the compressive strength was the lowest. Samples with square structure, for this material, showed the highest compressive strength and the lowest compressive modulus.

Bending strength tests of the honeycomb structure

Bending tests were performed on five samples for ULTEM9085, PA2200, and Digital ABS™ samples with triangular, square, and hexagonal structures, see Figures 20, 21, and 22. For reference, solid samples were printed from the same materials and compared with the honeycomb structures.

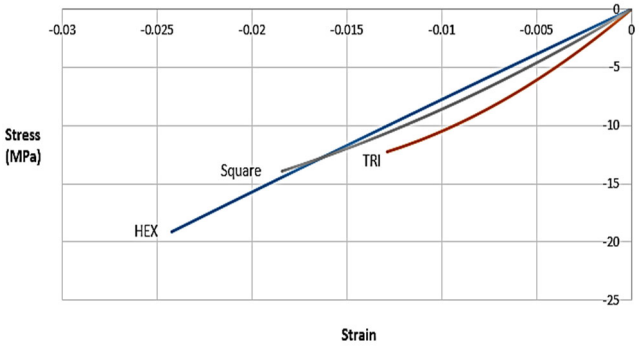

Fig. 20. ULTEM9085 structures stress-strain calculated from fit to bending data

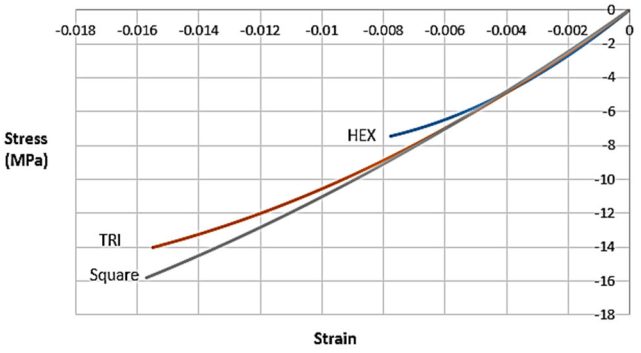

Fig. 21. PA2200 structures stress-strain calculated from fit to bending data

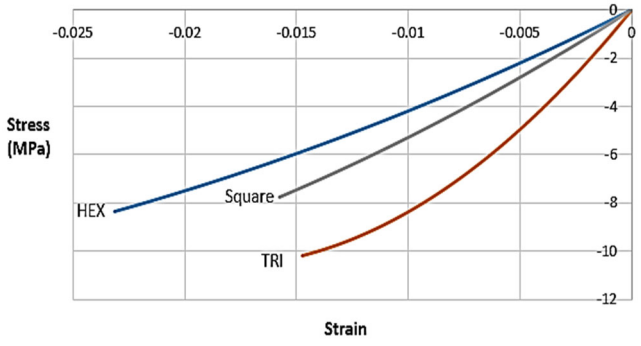

Fig. 22. Digital ABS™ structures stress-strain calculated from fit to bending data

The results from the bending tests show that the ULTEM9085 triangular structure has the highest value of flexural modulus and the lowest bending strength value. The hexagonal structure has the highest bending strength, but the lowest value of flexural modulus. In the case of PA2200, the hexagon structure has the highest value of flexural modulus, but the lowest bending strength value. The square structure has the highest bending strength but the lowest value of flexural modulus. Bending testing of Digital ABS™ hexagonal structure show that it has the lowest flexural modulus. The triangular structure has the highest bending strength, and the hexagonal and square structures have the same bending strength values.

4. Conclusions

3D bone models, solid (cortical), and void (trabecular) bone structures were designed, 3D printed, and tested. DICOM images from Computed Tomography (CT) scans

were used to create the bone structure for 3D printing. The resolution of these images did not allow the creation of fine trabecular bone structures, so we used 3D software for engineering special 3D void honeycomb structures.

Testing the mechanical properties of the honeycomb (triangular, square, and hexagonal) shows that their strength and modulus are higher than those of the real trabecular bones. Therefore, some of these materials can be used as a substitute/repair of the bones' trabecular part. On the other side, results from solid structures show that the 3D printed solid structures' strength was lower than the values of the cortical bone. Therefore, alternative solutions are needed to strengthen biopolymers (e.g. fibers and other particles to reinforce polymers have been investigated in different research). Further, specially designed external geometry for the solid part, together with honeycomb structures, can also increase the overall total strength of 3D printed bones.

Future research work proposed. We designed and built SLA (stereolithography) printer 3D with high resolution (10 micrometers) that can work without support material. Still, we could not find biocompatible resign that can work with that printer; and we are working on another research to formulate special ink/resin that supports such high resolution. Clearly, after reaching the mechanical properties of real bones, animal and clinical trials need to be performed to investigate their influence on healing bone structures.

References

[1] CT scan vs. MRI. Available from: http://www.diffen.com/difference/CT_Scan_vs_MRI (retrieved on 05/20/2020).

[2] Magnetic Resonance Imaging (MRI). Available from: http://www.webmd.com/a-to-z-guides/magnetic-resonance-imaging-mri (retrieved on 05/20/2020).

[3] A. Pugalendhi, M. Chandrasekaran, R. Ranganathan, Effect of process parameters on mechanical properties of VeroBlue material and their optimal selection in PolyJet technology, International Journal of Advanced Manufacturing Technology 108/1 (2020) 1049-1059. DOI: https://doi.org/10.1007/s00170-019-04782-z

[4] A Comprehensive Guide to Material Jetting 3D Printing. Available from: https://amfg.ai/2018/06/29/material-jetting-3d-printing-guide/ (retrieved on 05/20/2020).

[5] P. Ikonomov, A. Yahamed, Testing of plastic materials for 3D printing of bone structure, International Journal of Advanced Manufacturing Systems 15/1 (2014) 23-29.

[6] MeshLab, System for processing and editing 3D triangular meshes. Available from: https://www.meshlab.net/ (retrieved on 05/20/2020).

[7] S.I.A. Razak, N.F.A. Sharif, W.A.W.A. Rahman, Biodegradable polymers and their bone applications: a review, International Journal of Basic & Applied Sciences IJBAS-IJENS 12/1 (2012) 31-49.

[8] J.M. Williams, A. Adewunmi, R.M. Schek, C.L. Flanagan, P.H. Krebsbach, S.E. Feinberg, S.J. Hollister, S. Das, Bone tissue engineering using polycaprolactone scaffolds fabricated via selective laser sintering, Biomaterials 26/23 (2005) 4817-4827. DOI: https://doi.org/10.1016/j.biomaterials.2004.11.057

[9] T. Dikova, T. Vasilev, Bending fracture of Co-Cr dental bridges, produced by additive technologies: Simulation analysis and test, Engineering Fracture Mechanics 218 (2019) 106583. DOI: https://doi.org/10.1016/j.engfracmech.2019.106583

[10] A. Yahamed, P. Ikonomov, P.D. Fleming, A. Pekarovicova, P. Gustafson, Designed structures for bone replacement, Journal of Print and Media Technology Research 4-16 (2016) 267-350. DOI: https://doi.org/10.14622/JPMTR-1614

[11] C.T. Tao, T.H. Young, Polyetherimide membrane formation by the cononsolvent system and its biocompatibility of MG63 cell line, Journal of Membrane Science 269/1-2 (2006) 66-74. DOI: https://doi.org/10.1016/j.memsci.2005.06.019

[12] D.I. Stoia, C. Vigaru, L. Rusu, Laser sinterization aspects of PA2200 biocompatible powder – spinal cage application, Key Engineering Materials 638 (2015) 352-356. DOI: https://doi.org/10.4028/www.scientific.net/KEM.638.352